Journal of Power Sources 197 (2012) 292–296

Contents lists available at SciVerse ScienceDirect

Journal of Power Sources

journal homepage: www.elsevier.com/locate/jpowsour

Short communication

# Lithium redox behavior in *N*-methyl-*N*-propylpyrrolidinium bis(trifluoromethanesulphonyl)imide room temperature ionic liquid

Andrzej Lewandowski*, Agnieszka Swiderska-Mocek, Lukasz Waliszewski, Maciej Galinski

*Faculty of Chemical Technology, Poznań University of Technology, PL-60 965 Poznań, Poland*

ARTICLE INFO

*Article history:*
Received 27 July 2011
Received in revised form 24 August 2011
Accepted 27 August 2011
Available online 2 September 2011

*Keywords:*
Lithium
Electrode kinetics
Ionic liquid

ABSTRACT

The lithium metal–$Li^+$ interface was investigated in *N*-methyl-*N*-propylpyrrolidinium bis(trifluoromethanesulphonyl)imide room temperature ionic liquid, using impedance simulation, experimental electrochemical impedance spectroscopy (EIS) and scanning electron microscopy (SEM). The electrolyte contained vinylene carbonate as the solid electrolyte interphase (SEI) forming additive. The Warburg coefficient value obtained from impedance plot deconvolution ($A_W > 10\,\Omega\,s^{-1/2}$) and SEM lithium surface image suggest the SEI layer formation. Therefore, the charge transfer process on lithium reduction and oxidation takes place at the solid Li|SEI interface. Simulation studies show that the typical shape of impedance plots for the Li|$Li^+$ system (reported in the literature) suggests the exchange current density below $10^{-2}$ A cm$^{-2}$. The exchange current density of Li|SEI|$Li^+$ in the ionic liquid electrolyte, obtained from impedance spectra and Tafel plot is between $4.5 \times 10^{-4}$ A cm$^{-2}$ and $3.0 \times 10^{-4}$ A cm$^{-2}$ ($Li^+$ concentration of 0.7 mol dm$^{-3}$).



## 1. Introduction

Lithium reacts spontaneously and irreversibly with organic and inorganic liquid substances with the formation of a surface deposit of the reaction products [1]. The formed layer may passivate lithium and hence protects it against further corrosion. Due to its reactivity in contact with electrolytes, metallic lithium has been replaced by graphite as the anode material in Li-ion batteries [2]. However, in laboratory tests of a cathode or anode, lithium-metal is commonly used as both counter and reference electrodes. Moreover, metallic lithium may be used as a powerful reducing agent or as the anode in primary batteries. The importance of the passivation layer formed at lithium (nowadays called the solid electrolyte interface, SEI) for proper work of a lithium electrode was understood long ago [3] and SEI structure has been studied extensively [1,4–10]. Recently, room temperature ionic liquids (RTILs) have been studied as non-flammable electrolytes for Li-ion batteries [11,12]. Consequently, it is of great importance to study both kinetics and thermodynamics of the lithium/lithium(I) couple in ionic liquid electrolytes. Literature data concerning the role of passivation on the kinetics and thermodynamics of lithium oxidation to the $Li^+$ cation and the reverse reduction process [13–24] including studies in RTILs [25–27], are somewhat controversial. Some authors ignore the presence of the passive layer and interpret experimental results on the electrochemistry of the Li/$Li^+$ couple solely from the point of view of the charge transfer process, while some attribute Li/$Li^+$ couple properties mainly to the layer [20]. The general aim of the present paper was to investigate the role of SEI on kinetic parameters of lithium oxidation and $Li^+$ deposition in *N*-methyl-*N*-propylpyrrolidinium bis(trifluoromethanesulphonyl) imide ([MePrPyrr][$NTf_2$]).

## 2. Experimental

### 2.1. Materials

Lithium foil (0.75 mm thick, Aldrich), poly(acrylonitryle) (PAN, $M_W$ = 150 000, Aldrich), dimethylformamide (DMF, Aldrich), vinylene carbonate (VC, Aldrich) and lithium bis(trifluoromethanesulphonyl)imide ($LiNTf_2$, Fluka) were used as received. *N*-Methyl-*N*-propylpyrrolidinium bis(trifluoromethanesulphonyl) imide ([MePrPyrr][$NTf_2$]) was prepared according to the literature [28], by reacting N-methylpyrrolidinium (Aldrich) with propylbromide (Aldrich) followed by metathesis with lithium bis(trifluoromethanesulphonyl)imide. Liquid electrolyte was obtained by dissolution of solid $LiNTf_2$ in liquid $MePrPyrrNTf_2$ (0.7 M solution of $LiNTf_2$ in $MePrPyrrNTf_2$). Electrolytes contained VC as a SEI forming additive (10 wt.%) and were prepared in a dry argon atmosphere in a glove box. Polymer electrolytes were prepared by the casting technique. First, the polymer was swollen in DMF (50 °C). After 24 h the polymer solution was mixed with electrolyte (0.7 M $LiNTf_2$ in $MePrPyrrNTf_2$). The viscous solution

* Corresponding author. Tel.: +48 61 6652 309; fax: +48 61 6652 571.
*E-mail address:* andrzej.lewandowski@put.poznan.pl (A. Lewandowski).

0378-7753/$ – see front matter © 2011 Elsevier B.V. All rights reserved.
doi:10.1016/j.jpowsour.2011.08.109

of polymer in a mixture of the solvent and ionic liquid was cast onto a glass plate. After weighing, the plate was transferred into a desiccator where the solvent was slowly evaporated under a stream of dry argon, first at room temperature, then at 60 °C and finally at reduced pressure. After evaporation of the solvent, the plate with the polymer–electrolyte foil was weighed again and the composition of the electrolyte was determined from the mass balance. The polymer electrolyte composition: 31 wt.% polymer and 69 wt.% electrolyte (PAN 31 wt.%, $LiNTf_2$ 9.5 wt.%, $MePrPyrrNTf_2$ 59.5 wt.%).

### 2.2. Procedures and measurements

The Li/electrolyte/Li cells were assembled in a dry argon atmosphere in a glove box. Two lithium foils were separated by the glass micro-fibre GF/A separator (Whatmann) or polymer electrolyte (soaked with VC), placed in an adapted 0.5″ Swagelok® connecting tube. The surface area of Li electrodes was 0.79 $cm^2$. Electrochemical properties of the cells were characterized using electrochemical impedance spectroscopy (EIS) and galvanostatic charge–discharge tests. Interface resistance at the electrode/electrolyte interface was measured with an *ac* impedance analyzer (Atlas-Sollich System, Poland). The cycling measurements were done with the use of the μAutolab System (Eco Chemie, the Netherlands). Deconvolution of spectra was performed with the Z-view software (Scribner Associates Inc., USA). The glassy carbon electrode was initially (before the $j=f(E)$ measurements) covered with lithium (1 mA, 10 min). The Li/electrolyte/Li cells were polarized with a constant current (1 mA $cm^{-2}$) for 45 min and for the next 45 min at the opposite direction, in order to convert liquid VC into a solid SEI layer. Cyclic voltammetry measurements on a glassy carbon working electrode (0.0707 $cm^2$) were performed with a platinum foil counter electrode (1 $cm^2$). The reference electrode consisted of a silver wire immersed in a solution of $AgNTf_2$ and cryptand 222 in the solvent under study (Ag|$Ag^+$ 0.01 M, 222 0.1 M). Solutions of silver ions complexed by the cryptand ($Ag^+$222) were stable in contrast to those without the ligand. Potentials were then recalculated versus the lithium reference measured in the system: Ag|$Ag^+$ 0.01 M, 222 0.1 M||0.7 M $LiNTf_2$, $MePrPyrrNTf_2$, VC|Li. Scanning electron microscopy (SEM) of the lithium electrode was performed with the Tescan Vega 5153 apparatus.

## 3. Results and discussion

### 3.1. Impedance simulation

Simulation of impedance plots was performed for two equivalent circuits (Figs. 1A and 2A) and the selected electrolyte conductivity as well as $Li^+$ diffusion constant, for different charge transfer resistance (exchange current density).

#### 3.1.1. Electrolyte resistance

For electrolytes of low conductivity ($\sigma \approx 1.5$–2 mS $cm^{-2}$), the typical separator thickness of ca. 0.5 mm, and the lithium electrode surface of ca. 1 $cm^2$, the resistance is $R_{el} = (\sigma^{-1}/(l/A)) \approx 30\,\Omega$. Conductivity of lithium salts in cyclic carbonates is considerably higher (order of 10–14 mS $cm^{-1}$ [29]) and consequently, electrolyte resistance is much lower (ca. 3 Ω).

#### 3.1.2. $Li^+$ diffusion impedance

The Warburg impedance $Z_W$ is a reciprocal of the frequency square root $\sqrt{\omega}$:

$$Z_W = \frac{A_W}{\sqrt{\omega}} - i\frac{A_W}{\sqrt{\omega}} \quad (1)$$

where i is the imaginary unit ($i = \sqrt{-1}$).

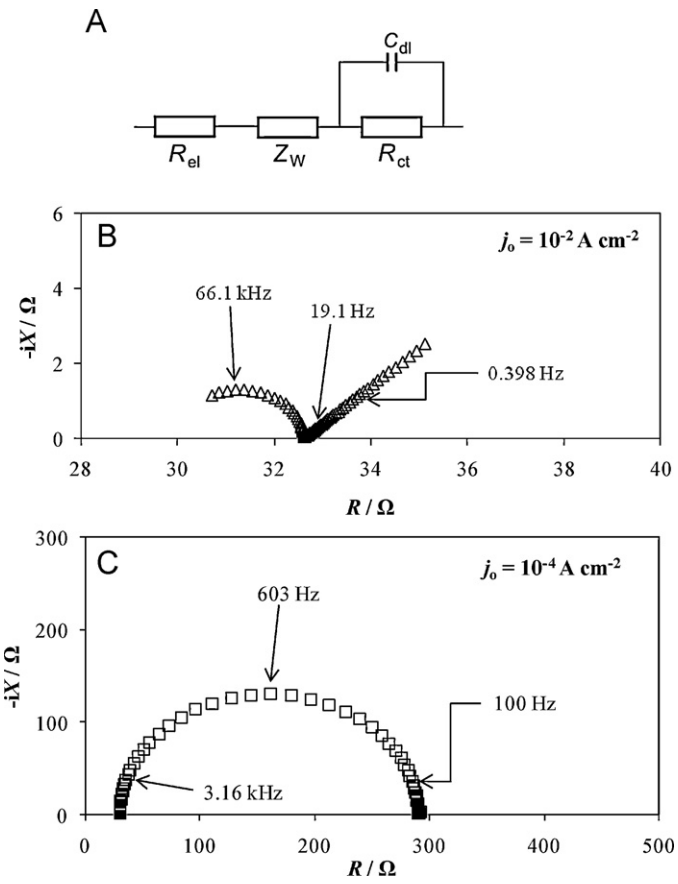


**Fig. 1.** Simulation of impedance spectra for the Li/$Li^+$ system (without the SEI layer), accordingto equivalent circuit (A). Data calculated for electrolyte resistance $R_{el} = 30\,\Omega$, Warburg constant $A_W = 2\,\Omega\,s^{-1/2}$, capacitance $C_{dl} = 1 \times 10^{-6}$ F and different charge transfer resistances (B): $R_{ct} = 2.6\,\Omega$ ($j_o = 10^{-2}$ A $cm^{-2}$) and (C) $R_{ct} = 260\,\Omega$ ($j_o = 10^{-4}$ A $cm^{-2}$).

The proportionality constant $A_W$ depends on the depolarizer concentration $c$ and diffusion constant $D$:

$$A_W \approx \frac{RT}{F^2 A\sqrt{2}}\left(\frac{1}{\sqrt{Dc}}\right) = 1.88 \times 10^{-7}\left(\frac{1}{\sqrt{Dc}}\right)\frac{\Omega}{\sqrt{s}} \quad (2)$$

where $T$, $R$ and $F$ are temperature, gas constant and Faraday constant, respectively, when $D$ is expressed in $cm^2\,s^{-1}$ and $c$ in mol $cm^{-3}$.

The typical value of the $Li^+$ diffusion coefficient in molecular solvents is of the order of $10^{-6}$ $cm^2\,s^{-1}$ ($D(LiClO_4$ in PC) = $3.99 \times 10^{-6}$ $cm^2\,s^{-1}$ [18], $D(Li^+$ in DMC) = $1.1 \times 10^{-6}$ $cm^2\,s^{-1}$ [22], $D(Li^+$ in THF) = $8.7 \times 10^{-6}$ $cm^2\,s^{-1}$ [24]) which leads to the value of $A_W = 0.19\,\Omega\,s^{-1/2} \approx 0.2\,\Omega\,s^{-1/2}$ (for $[Li^+] = 1\,M = 10^{-3}$ mol $cm^{-3}$). However, in the case of ionic liquids the diffusion coefficient is typically two orders of magnitude lower ($D(Li^+$ in ILs) $\approx 10^{-8}$ $cm^2\,s^{-1}$ [11,26,27,30]), which leads to $A_W$ values of the order of $2\,\Omega\,s^{-1/2}$. Therefore, the reduction of the $Li^+$ cation from the liquid electrolyte ($10^{-6}$ $cm^2\,s^{-1} < D < 10^{-8}$ $cm^2\,s^{-1}$) at the Li|$Li^+$ interphase, results in the $A_W$ parameter between $0.2\,\Omega\,s^{-1/2}$ and $2\,\Omega\,s^{-1/2}$ (for the electrode surface of 1 $cm^2$). On the other hand, if the SEI layer is formed, the reduction process takes place at a solid|solid interphase: Li|SEI|$Li^+$. Diffusion coefficient of the $Li^+$ cation in the solid state is much lower in comparison to that characteristic of the liquid phase. To our knowledge there is no consistent set of data on the $Li^+$ diffusion coefficient in SEI in the literature. Moreover, SEI structure and composition depend on the electrolyte and are dynamic during electrode charging/discharging [8]. Even data for $Li^+$ diffusion in well-defined

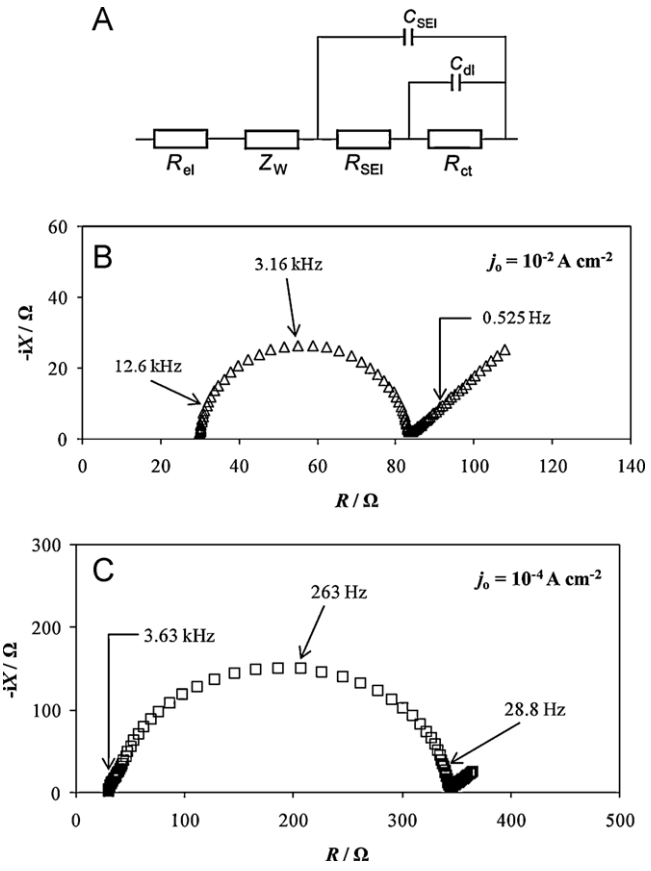


**Fig. 2.** Simulation of impedance spectra for the Li/Li$^+$ system (with the SEI layer), according to equivalent circuit (A). Data calculated for electrolyte resistance $R_{el} = 30\,\Omega$, Warburg constant $A_W = 20\,\Omega\,s^{-1/2}$, capacitances: $C_{dl} = 1 \times 10^{-6}$ F, $C_{SEI} = 1 \times 10^{-6}$ F and different charge transfer resistances (B): $R_{ct} = 2.6\,\Omega$ ($j_o = 10^{-2}$ A cm$^{-2}$) and (C) $R_{ct} = 260\,\Omega$ ($j_o = 10^{-2}$ A cm$^{-2}$). Resistance of the SEI layer: $R_{SEI} = 50\,\Omega$.

materials are not consistent. For example, $D$(Li) in graphite, measured with different methods, is contained within a broad range of $10^{-6}$–$10^{-14}$ cm$^2$ s$^{-1}$ [31–33]. The corresponding data for lithium diffusion in $LiFePO_4$ are $10^{-11}$ cm$^2$ s$^{-1}$ < $D$(Li) < $10^{-15}$ cm$^2$ s$^{-1}$ [34,35] and $10^{-11}$ cm$^2$ s$^{-1}$ < $D$(Li) < $10^{-12}$ cm$^2$ s$^{-1}$ in $LiCoO_2$ [36]. Typical solid-state diffusion coefficients of $10^{-10}$ cm$^2$ s$^{-1}$ and $10^{-11}$ cm$^2$ s$^{-1}$ (middle of the range) lead to the corresponding $A_W$ values of 20 Ω s$^{-1/2}$ and 60 Ω s$^{-1/2}$, respectively.

### 3.1.3. Charge transfer resistance

In the literature the kinetics of the charge transfer reaction is described by exchange current density, $j_o$, rate constant $k_o$ or corresponding resistance $R_{ct}$, which are mutually related according to Eqs. (3) and (4):

$$j_o = \frac{RT}{F}\frac{1}{R_{ct}} \quad (3)$$

and

$$j_o = Fk_o[Li^+] \quad (4)$$

Typical values of $j_o$, obtained from voltammetry, are between $10^{-2}$ A cm$^{-2}$ and $10^{-4}$ A cm$^{-2}$, which leads to charge transfer resistances of 2.6 and 260 Ω (for electrode surface of 1 cm$^2$).

### 3.1.4. Nyquist plot simulation

Fig. 1 shows simulation of the impedance spectrum (frequencies in the range of $10^5$–0.01 Hz) for the Li|Li$^+$ system (without SEI formation), approximated by the simple equivalent circuit (Fig. 1A), consisting of electrolyte ($R_{el}$) and charge transfer ($R_{ct}$) resistances as well as Warburg impedance ($Z_W$) due to Li$^+$ diffusion. Data for the Li|Li$^+$ system were calculated for electrolyte resistance $R_{el} = 30\,\Omega$, Warburg constant $A_W = 2\,\Omega\,s^{-1/2}$ and different charge transfer resistances (B): $R_{ct} = 2.6\,\Omega$ and (C) $R_{ct} = 260\,\Omega$ (capacitance of the double layer was $10^{-6}$ F). It can be seen that in the case of fast kinetics ($j_o = 10^{-2}$ A cm$^{-2}$, $R_{ct} = 2.6\,\Omega$), the impedance spectrum consists of a half-semicircle followed by a line, while the corresponding curve for slower rates ($j_o = 10^{-4}$ A cm$^{-2}$, $R_{ct} = 260\,\Omega$) is a semicircle. To our knowledge, the first type of impedance spectrum (Fig. 1B) has not been reported for the Li|Li$^+$ system. Fig. 2 shows the simulation of the corresponding impedance plot for a system, where formation of SEI was taken into account (Li|SEI|Li$^+$ system). The equivalent circuit consists of two *RC* systems, one representing the SEI layer, the other the charge transfer process (Fig. 2A). Resistance of the SEI layer was approximated by value of ca. 50 Ω and capacitance of both SEI and the double layer by $10^{-6}$ F. The shape of both curves, calculated for the same electrolyte resistance and Warburg constant ($R_{el} = 30\,\Omega$, $A_W = 20\,\Omega\,s^{-1/2}$) and different kinetic parameters ($R_{ct} = 2.6\,\Omega$ or 260 Ω) is a semicircle. In the case of the faster kinetics ($j_o = 10^{-2}$ A cm$^{-2}$, $R_{ct} = 2.6\,\Omega$) the semicircle is followed by a straight line (Fig. 2B). Again, impedance spectra reported in the literature consist of a semicircle without a straight line at lower frequencies or with a short line [4,15–17,21,29,37–44]. All this indicates that impedance data point to relatively slow kinetics ($j_o \ll 10^{-2}$ A cm$^{-2}$).

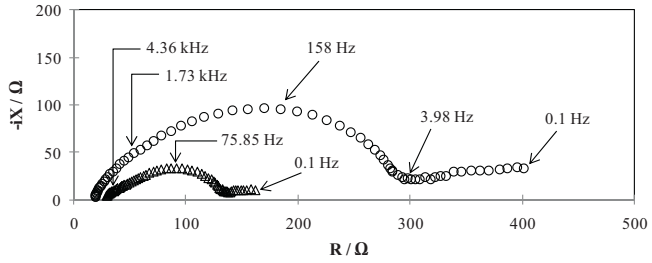


**Fig. 3.** Impedance spectra of the symmetrical, two electrode Li|0.7 M $LiNTf_2$ + $MePrPyrrNTf_2$ + 10 wt.% VC|Li cell; (○) immediately after assembling and (△) after galvanostatic charging/discharging (1 mA). Lithium electrodes area: 0.79 cm$^2$ and electrolyte volume: 0.09 cm$^3$.

### 3.2. Experimental studies of the Li|Li$^+$ couple

Fig. 3 shows impedance spectra of the symmetrical, two electrode Li|0.7 M $LiNTf_2$ in the $MePrPyrrNTf_2$ + 10 wt.% VC|Li cell just after its assembling and after galvanostatic charging/discharging (1 mA cm$^{-2}$, 45 min each step, electrode surface 0.79 cm$^2$). It can be seen that impedance spectra consist of flat semicircles, followed by a line due to the diffusion of lithium ions. The semicircle may be deconvoluted into two separate semicircles, representing the SEI layer and charge transfer resistances. The cell just after its assembling is characterized by relatively high impedance due to metallic-lithium corrosion in the electrolyte, with the formation of a resistive layer. During charging and discharging processes the SEI layer is electrochemically formed which results in a significant impedance decrease. The shape of both curves is similar to that shown in Fig. 2C.

### 3.2.1. Diffusion impedance

The value of Warburg coefficient, $A_W$, obtained from impedance plot deconvolution, is ca. 70 Ω s$^{-1/2}$ for the fresh cell and 17 Ω s$^{-1/2}$ after charging/discharging. This may suggest that the diffusion coefficient is lower than $10^{-10}$ cm$^2$ s$^{-1}$, and hence, indicates the formation of a solid electrolyte|electrode interphase. Changes of

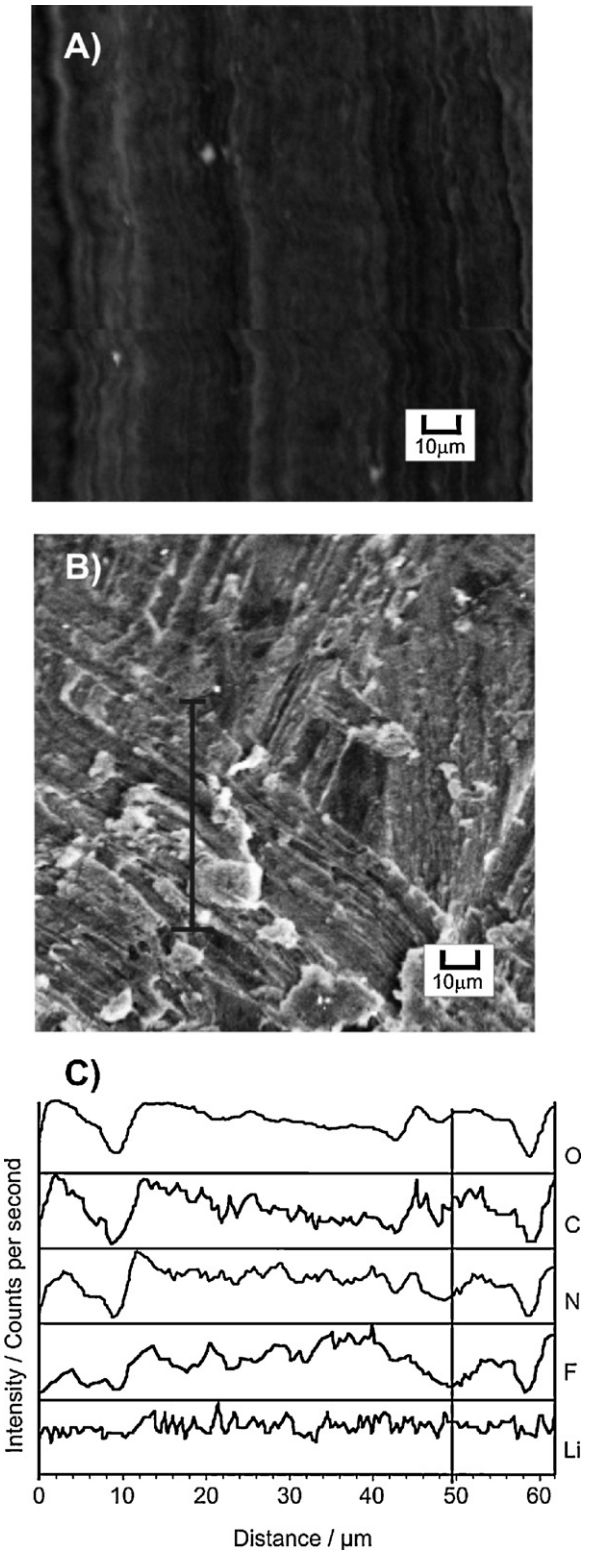


**Fig. 4.** SEM images of the metallic-lithium anode: (A) a pristine electrode (B) after 5th charge/discharge cycles and (C) EDX analysis of the cycled anode. Polymer electrolyte composition (before cycling): $LiNTf_2$ (8.9 wt.%), $MePrPyrrNTf_2$ (55.7 wt.%), PAN (29.2 wt.%), and VC (6.2 wt.%).

lithium surface after electrochemical charging/discharging are suggested by scanning electron microscopy. Fig. 4 shows SEM images of (A) a pristine metal–lithium electrode after contact with the polymer electrolyte based on ionic liquid (4 h) and (B) after its electrochemical cycling (5 cycles). The SEM image was taken with

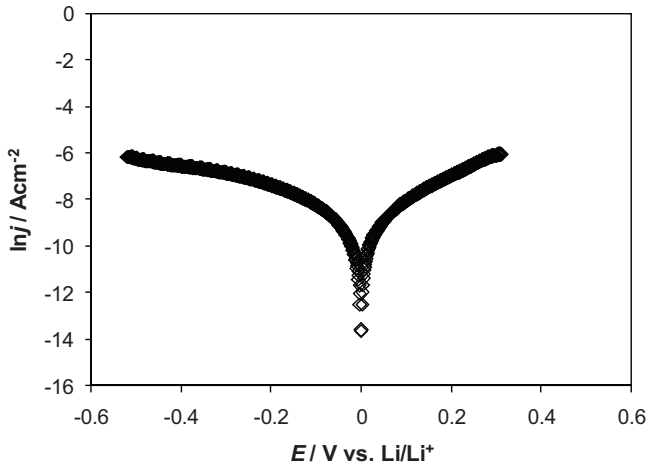


**Fig. 5.** The Tafel plot for the GC|0.7 M $LiNTf_2$ and $MePrPyrrNTf_2$ + 10 wt.% VC system. Working electrode: glassy carbon (GC, 0.0707 $cm^2$) and counter electrode: Pt (1 $cm^2$). Scan rate: 1 mV $s^{-1}$.

electrodes working with the polymer electrolyte, in order to avoid traces of separator threads on the electrode surface. It can be seen in Fig. 4B that during electrochemical charging/discharging the flat lithium foil was covered with aggregates. This is not unexpected as processes of SEI formation lead to a coverage of the anode in multilayer surface films which are comprised of organic and inorganic (lithium salts) molecules [5] with non-smooth or nano-rough surface [7,45]. The thickness of SEI is small and hence investigation of its composition is limited to a few techniques, each with its limitations [7]. Fig. 4C shows EDX analysis of the cycled anode, indicating composition of the surface layer (Li, C, O, N, F). Inorganic salts are composed of Li, F and O ($Li_2CO_3$, $Li_2O$, LiF, etc.) while the organic phase generally consists of C, O and N [5].

### 3.2.2. Charge transfer kinetics

Deconvolution of impedance data for the system with electrochemically formed SEI (shown graphically in Fig. 3) leads to $R_{el}$, $R_{SEI}$ and $R_{ct}$ values. The electrolyte resistance is $R_{el} = 31\,\Omega$. The corresponding value for the thin SEI layer formed at the lithium electrode, is almost identical ($R_{SEI} = 30\,\Omega$). This indicates very low specific conductivity of the SEI. The resistance of the charge transfer process is $R_{ct} = 68\,\Omega$. The charge transfer resistance is equivalent to exchange current density (at 298 K) of $j_o = 0.026\,V/(68\,\Omega \times 0.79\,cm^2) = 4.8 \times 10^{-4}\,A\,cm^{-2}$. A similar value of $j_o = 3.0 \times 10^{-4}\,A\,cm^{-2}$ was detected from the Tafel plot (Fig. 5). It is difficult to calculate concentration independent rate constant $k_o$, as the charge transfer process occurs at the interface between two solid SEI|Li phases and not at the electrolyte|$Li^+$(electrolyte) interface.

Kinetic data obtained in this work for the lithium reduction in $MePrPyrrNTf_2$ may be compared with literature data derived with the use of EIS and voltammetric techniques in a range of classical electrolytes in molecular solvents, ionic liquids and polymer electrolytes. However, the comparison may be difficult due to the variety of electrode materials, the chemical character of solvents and anions, and different experimental conditions. Different electrodes were used: lithium amalgam [13], metallic-lithium [4,15–17,20,29], platinum [18,19,24,26], graphite [46,47], tungsten [22,25], stainless steel [36] and nickel [23,26,27]. Experimental methods were based on the Tafel plot [13,15,17], EIS curve deconvolution [29], the analysis of cyclic voltammetry curves (Allen–Hückling equation [18,19,23] or numerical simulation [24,26,27]) and voltammetry on a rotating disc electrode [48].

Lithium salts were based on different anions ($Cl^-$, $ClO_4^-$, $PF_6^-$, $AsF_6^-$, $BF_4^-$, $CF_3SO_3^-$, $N(CF_3SO_2)_2^-$). Moreover, kinetic characteristics of the $Li^+$ reduction are reported as concentration dependent $R_{ct}$, $j_o$ values or the concentration independent rate constant $k_o$. The latter parameter obtained for $Li^+$ reduction in molecular liquids is $k_o$(DMSO, Hg(Li) electrode) = $2.9 \times 10^{-5}$ cm s$^{-1}$ [13] and $k_o$(THF) = $1 \times 10^{-4}$ cm s$^{-1}$ [24]. In the case of a number of ionic liquids the rate constant is of the order of $1 \times 10^{-5}$ cm s$^{-1}$ [26,27]. More papers report the concentration dependent $j_o$ value, which is in the broad range of $10^{-2}$–$10^{-4}$ A cm$^{-2}$ [17–19,48] at concentrations typically of 1–0.1 mol dm$^{-3}$. Generally, the experimental EIS curves (Fig. 3) have different shape in comparison to simulated impedance spectra, calculated according to equivalent circuit without SEI layer (Fig. 1) in contrast to those with SEI (Fig. 2). This strongly suggests SEI formation. In addition, experimental EIS curves resembles rather simulated curve shown in Fig. 2C, which indicates rather low kinetics ($j_o$ at the order of $10^{-4}$ A cm$^{-2}$).

## 4. Conclusions

The Warburg coefficient value obtained from impedance plot deconvolution ($A_W > 10\ \Omega\ s^{-1/2}$) and SEM lithium surface image suggest SEI layer formation. Therefore, the charge transfer process on lithium reduction and oxidation takes place at the solid Li|SEI interphase and not at the Li|electrolyte surface. Simulation studies show that the typical shape of impedance plots for the Li|$Li^+$ system (reported in the literature) suggest the exchange current density much lower than $10^{-2}$ A cm$^{-2}$. The exchange current density of the Li|SEI|$Li^+$ system in the ionic liquid electrolyte, obtained from impedance spectra and the Tafel plot is between $4.5 \times 10^{-4}$ A cm$^{-2}$ and $3.0 \times 10^{-4}$ A cm$^{-2}$ ($Li^+$ concentration of 0.7 mol dm$^{-3}$).

## Acknowledgement

Support of grant DS31-225/10 is gratefully acknowledged.

## References

[1] D. Rahner, S. Machill, K. Siury, J. Power Sources 68 (1997) 69–74.
[2] R. Yazami, P. Touzain, J. Power Sources 9 (1983) 365–371.
[3] A. Dey, Thin Solid Films 43 (1977) 131–171.
[4] A. Zaban, E. Zinigrad, D. Aurbach, J. Phys. Chem. 100 (1996) 3089–3101.
[5] D. Aurbach, J. Power Sources 89 (2000) 206–218.
[6] F. Kong, R. Kostecki, G. Nadeau, X. Song, K. Zaghib, K. Kinoshita, F. McLarnon, J. Power Sources 98 (2001) 58–66.
[7] K. Edström, M. Herstedt, D.P. Abraham, J. Power Sources 153 (2006) 380–384.
[8] H. Bryngelsson, M. Stjerndahl, T. Gustafsson, K. Edström, J. Power Sources 174 (2007) 970–975.
[9] J. Yan, B.-J. Xia, Y.-C. Su, X.-Z. Zhou, J. Zhang, X.-G. Zhang, Electrochim. Acta 53 (2008) 7069–7078.
[10] J. Yan, Y.-C. Su, B.-J. Xia, J. Zhang, Electrochim. Acta 54 (2009) 3538–3542.
[11] M. Galinski, A. Lewandowski, I. Stepniak, Electrochim. Acta 51 (2006) 5567–5580.
[12] A. Lewandowski, A. Świderska-Mocek, J. Power Sources 194 (2009) 601–609.
[13] D.R. Cogley, J.N. Butler, J. Phys. Chem. 72 (1968) 4568–4573.
[14] C.A.C. Sequeira, A. Hooper, Solid State Ionics 9–10 (1983) 1131–1138.
[15] G. Nagasubramanian, A.I. Attia, G. Halpert, J. Appl. Electrochem. 24 (1994) 298–302.
[16] D. Rahner, S. Machill, G. Ludwig, J. Power Sources 54 (1995) 378–382.
[17] C. Liebenow, K. Lühder, J. Appl. Electrochem. 26 (1996) 689–692.
[18] X.-M. Wang, T. Nishina, I. Uchida, J. Power Sources 68 (1997) 483–486.
[19] X.-M. Wang, M. Iyoda, T. Nishina, I. Uchida, J. Power Sources 68 (1997) 487–491.
[20] N. Munichandraiah, A.K. Shukla, L.G. Scanlon, R.A. Marsh, J. Power Sources 62 (1996) 201–206.
[21] N. Munichandraiah, L.G. Scanlon, R.A. Marsh, J. Power Sources 72 (1998) 203–210.
[22] A. Chausse, M. Berhil, R. Messina, Electrochim. Acta 44 (1999) 2365–2370.
[23] Y. Kato, T. Ishihara, Y. Uchimoto, M. Wakihara, J. Phys. Chem. B 108 (2004) 4794–4798.
[24] C.A. Paddon, S.E. Ward Jones, F.L. Bhatti, T.J. Donohoe, R.G. Compton, J. Phys. Org. Chem. 20 (2007) 677–684.
[25] P.-Y. Chen, J. Chin. Chem. Soc. 53 (2006) 1017–1026.
[26] R. Wibowo, S.E. Ward Jones, R.G. Compton, J. Phys. Chem. B 113 (2009) 12293–12298.
[27] R. Wibowo, S.E. Ward Jones, R.G. Compton, J. Chem. Eng. Data 55 (2010) 1374–1376.
[28] A. Lewandowski, A. Swiderska-Mocek, J. Power Sources 194 (2009) 502–507.
[29] C. Fringant, A. Tranchant, R. Messina, Electrochim. Acta 40 (1995) 513–523.
[30] P.L. Allen, A. Hickling, Trans. Faraday Soc. 53 (1957) 1626–1635.
[31] P. Yu, B.N. Popov, J.A. Ritter, R.E. White, J. Electrochem. Soc. 146 (1999) 8–14.
[32] M. Umeda, K. Dokko, Y. Fujita, M. Mohamedi, I. Uchida, J.R. Selman, Electrochim. Acta 47 (2001) 885–890.
[33] Y. NuLi, J. Yang, Z. Jiang, J. Phys. Chem. Solids 67 (2006) 882–886.
[34] Y.-R. Zhu, Y. Xie, R.-S. Zhu, J. Shu, L.-J. Jiang, H.-B. Qiao, T.-F. Yi, Ionics 17 (2011) 437–441.
[35] W.L. Liu, J.P. Tu, Y.Q. Qiao, J.P. Zhou, S.J. Shi, X.L. Wang, C.D. Gu, J. Power Sources 196 (2011) 7728–7735.
[36] H. Xia, L. Lu, G. Ceder, J. Power Sources 159 (2006) 1422–1427.
[37] C. Sirisopanaporn, A. Fernicola, B. Scrosati, J. Power Sources 186 (2009) 490–495.
[38] M. Egashira, H. Todo, N. Yoshimoto, M. Morita, J.-I. Yamaki, J. Power Sources 174 (2007) 560–564.
[39] A. Fernicola, F. Croce, B. Scrosati, T. Watanabe, H. Ohno, J. Power Sources 174 (2007) 342–348.
[40] H. Sakaebe, H. Matsumoto, K. Tatsumi, J. Power Sources 146 (2005) 693–697.
[41] N. Byrne, P.C. Howlett, D.R. MacFarlane, M. Forsyth, Adv. Mater. 17 (2005) 2497–2501.
[42] G.-T. Kim, G.B. Appetecchi, F. Alessandrini, S. Passerini, J. Power Sources 171 (2007) 861–869.
[43] J.-K. Kim, G. Cheruvally, X. Li, J.-H. Ahn, K.-W. Kim, H.-J. Ahn, J. Power Sources 178 (2008) 815–820.
[44] J-W. Choi, G. Cheruvally, Y.H. Kim, J-K. Kim, J. Manuel, P. Raghavan, J-H. Ahn, K-W. Kim, H-J. Ahn, D.S. Choi, C.E. Song, Solid State Ionics 178 (2007) 1235–1241.
[45] H. Buqa, P. Golob, M. Winter, J.O. Besenhard, J. Power Sources 97–98 (2001) 122–125.
[46] M.D. Levi, D. Aurbach, J. Phys. Chem. B 101 (1997) 4630–4640.
[47] Y. Yamada, Y. Iriyama, T. Abe, Z. Ogumi, Langmuir 25 (2009) 12766–12770.
[48] S.-I. Lee, U.-H. Jung, Y.-S. Kim, M.-H. Kim, D.-J. Ahn, H.-S. Chun, Korean J. Chem. Eng. 19 (2002) 638–644.